Detection of Double JPEG Compression With the Same Quantization Matrix via Convergence Analysis

Yakun Niu, Xiaolong Li, Yao Zhao, *Senior Member, IEEE*, and Rongrong Ni

***Abstract*— Detecting double JPEG compression with the same quantization matrix is a challenging task in image forensics. To address this problem, in this paper, a novel method is proposed by leveraging the component convergence during repeated JPEG compressions. Firstly, an in-depth analysis of the pipeline in successive JPEG compressions is conducted, and it reveals that the rounding/truncation errors as well as JPEG coefficients tend to converge after multiple recompressions. Based on this fact, the backward quantization error (BQE) is defined, and we find that the ratio of non-zero BQE for single compression is larger than that for double compression. Moreover, to exploit the convergence property of JPEG coefficients, a multi-threshold strategy is designed for capturing the statistics of the number of different JPEG coefficients between two sequential compressions. Finally, the statistical features of the dual components are concatenated into a 15-D vector to detect double JPEG compression. Experimental results demonstrate the efficiency of the proposed method, which outperforms some state-of-the-art schemes.**

***Index Terms*— Image forensics, double JPEG compression, rounding/truncation errors, JPEG coefficients.**

I. Introduction

IDENTIFYING the originality and authenticity of digital images is challenging nowadays since forgery becomes a rather convenient and simple task, even for non-professional users. If maliciously forged images are abused, it can be a serious problem for our community security. Fortunately, researchers have developed a variety of approaches to inspect the image integrity [1]–[7]. Many of them operate by directly identifying traces of manipulation since it usually inevitably leaves unique fingerprints on images. Detecting manipulation, such as median filtering [8]–[11], resampling [12]–[15], contrast enhancement [16]–[18], and JPEG compression [19]–[22], involved in image tampering not only reveals the forgery but also recovers the image processing history.

Manuscript received April 3, 2021; revised June 13, 2021; accepted July 3, 2021. Date of publication July 15, 2021; date of current version May 5, 2022. This work was supported in part by the National Key Research and Development Program of China under Grant 2020AAA0140003 and in part by the National Natural Science Foundation of China under Grant U1936212. This article was recommended by Associate Editor Z. Li. *(Corresponding author: Yao Zhao.)*

The authors are with the Institute of Information Science, Beijing Jiaotong University, Beijing 100044, China, and also with the Beijing Key Laboratory of Advanced Information Science and Network Technology, Beijing 100044, China (e-mail: niuyakun@bjtu.edu.cn; lixl@bjtu.edu.cn; yzhao@bjtu.edu.cn; rrni@bjtu.edu.cn).

Color versions of one or more figures in this article are available at https://doi.org/10.1109/TCSVT.2021.3097351.

Digital Object Identifier 10.1109/TCSVT.2021.3097351

Double JPEG compression detection plays a major role in image forensics since double compression is inevitable when a JPEG image forgery is created [23]–[28]. This detection task has two cases: double JPEG compression with different quantization matrices and that with the same quantization matrix. For the first case, some effective methods have been proposed [29]–[37]. In [29], Lukas and Fridrich proposed to explore the local peaks and missing values in the JPEG coefficients histogram. In [30], Popescu and Farid demonstrated that double JPEG compression can be detected by measuring the periodic artifacts of JPEG coefficients histograms via Fourier transform. In [31], Fu *et al.* observed that the first digits distribution of AC coefficients for singly compressed image follows a generalized Benford's law, which can be utilized for double JPEG compression detection. In [32], Li *et al.* as an extension of [31], Fu *et al.* proposed to use the first digits of JPEG coefficients from some specifically selected AC channels. In [33], the transition probability matrices derived from the difference JPEG 2-D arrays are utilized. Recently, unlike the aforementioned hand-craft features based methods, several CNN based methods [34]–[37] have been proposed. In [34], the concatenated DCT histograms are taken as the input of CNN. In [35], CNN is trained directly with the images in both the pixel and noise domains. In [36], considering both the spatial and frequency domains, a multi-domain based approach is proposed with CNN. In [37], the quantization table is considered to facilitate the detection with mixed quality factors (QFs). At present, for the case of double JPEG compression detection with different quantization matrices, high accuracy performance can be achieved, even for small image patches.

However, the aforementioned methods [29]–[37] would fail to detect double JPEG compression with the same quantization matrix. To the best of our knowledge, only a few works have focused on this task. In [38], Huang *et al*. observed that the number of different JPEG coefficients (NDC) between two sequential compressed images decreases in successive JPEG compressions. Based on this observation, a random perturbation strategy is designed to obtain an image dependent threshold, then by comparing the threshold with NDC, double JPEG compression can be identified. In [39], Yang *et al*. found that during JPEG compression, for the image block in which rounding or truncation error exists, the maximal and average errors of single compression are larger than those of double compression. Then, the variance and mean of rounding

and truncation error blocks are used to extract features for detection. In our previous work [40], for improving [38], a novel random perturbation strategy based detection method is proposed. Unlike Huang *et al.*'s work that indiscriminately selects JPEG coefficients for modification, only coefficients valued ± 1 are modified with a novel strategy. Recently, several CNN based methods have been proposed as well for this detection task [41]–[43]. Although considerable progress has been made, most of existing methods do not make full use of the statistical difference between single and double JPEG compressions, that degrades the detection performance, especially for the case of low QFs. Furthermore, there is a lack of theoretical analysis of the rounding/truncation errors and JPEG coefficients in successive JPEG compressions. Filling in these gaps will promote the detection accuracy.

In this paper, a novel method is proposed to detect double JPEG compression with the same quantization matrix. Firstly, an in-depth analysis of the pipeline in successive JPEG compressions is conducted and it derives that rounding/truncation errors as well as JPEG coefficients tend to converge after multiple recompressions. Based on this fact, the backward quantization error (BQE) is defined, and we find that the ratio of non-zero BQE for single compression is larger than that for double compression. Then, a set of such ratios (named error-based features) is respectively extracted from rounding and truncation error blocks. Moreover, a multi-threshold strategy (MTS) is designed to exploit the convergence property of JPEG coefficients. Specifically, a novel perturbation strategy is proposed, in which multiple thresholds are derived with different modification ratios on JPEG coefficients. Then, the differences between the multiple thresholds and NDC (called perturbation-based features) are utilized as features. Finally, the error- and perturbation-based features are concatenated into a 15-D vector for detection. Extensive experimental results demonstrate that the proposed method provides superior performance to some state-of-the-art works [38]–[40].

The rest of this paper is organized as follows. In Section II, the problem statement and the motivation for double JPEG compression detection are reported. Section III mainly introduces the proposed method leveraging the convergent rates of rounding/truncation errors and JPEG coefficients to detect double JPEG compression. Experimental results are presented in Section IV and the conclusion is drawn in Section V.

II. Preliminary

A. Problem Statement

The JPEG compression procedure, including compression and de-compression phases, is shown in Fig. 1. In the compression phase, a raw image is first split into non-overlapping 8×8 blocks, and each image block X^1 is then performed with DCT to obtain its corresponding transformed block

$$Y^1 = \mathrm{DCT}(X^1). \tag{1}$$

Next, the transformed block is component-wisely divided by the quantization steps and then rounded to yield the JPEG coefficients block $[Y^1/Q]$. Here, $[\cdot]$ denotes the rounding

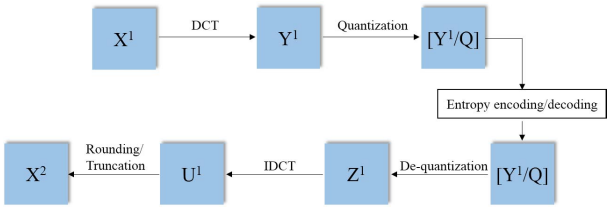

Fig. 1. JPEG compression procedure.

operation and Q is the 8×8 quantization matrix consisting of 64 quantization steps $q_i \in \mathbb{N}$ with $i \in \{0, \ldots, 63\}$. Finally, lossless entropy encoding is performed on JPEG coefficients to derive the compressed bitstream.

In JPEG de-compression phase, after entropy decoding, the JPEG coefficients are component-wisely multiplied by Q to obtain the de-quantized JPEG coefficients

$$Z^1 = \left[\frac{Y^1}{Q}\right] Q. \tag{2}$$

Then, the inverse DCT (IDCT) is performed on Z^1 to bring the coefficients back to the spatial domain to derive the de-transformed block

$$U^1 = \mathrm{IDCT}(Z^1). \tag{3}$$

Finally, each element of U^1 is rounded to its nearest integer and then truncated in the range of $[0, 255]$ to obtain the de-compressed image block

$$X^2 = \mathrm{RT}(U^1). \tag{4}$$

Here, $\mathrm{RT}(\cdot)$ means the rounding and truncation operations.

Notice that, in JPEG compression procedure, three types of information loss, namely quantization, rounding and truncation errors, are generated. Quantization and rounding errors always exist, while truncation error does not. The quantization error occurs within quantization and de-quantization operations (Q&D), while the rounding error is generated in the final step of JPEG compression, in which U^1 should be rounded to integers. Then, if $X^2 \neq [U^1]$, the truncation error occurs and the block is called truncation error block. Otherwise, i.e., $X^2 = [U^1]$, the block is simply rounded without truncation operation, and it is called rounding error block.

Repeating the above compression and de-compression phases on each image block X^2, the doubly compressed image with the same quantization matrix Q is thus obtained. For clarity, considering repeated compressions and de-compressions for k times, in the same way, we respectively define X^k, Y^k, Z^k and U^k as the image block, transformed block, de-quantized JPEG coefficients block, and de-transformed block. Specifically, with a given raw image block X^1, these blocks can be sequentially computed as follows for each $k \geq 1$

$$\begin{cases} Y^k = \mathrm{DCT}(X^k) \\ Z^k = [Y^k/Q]Q \\ U^k = \mathrm{IDCT}(Z^k) \\ X^{k+1} = \mathrm{RT}(U^k). \end{cases} \tag{5}$$

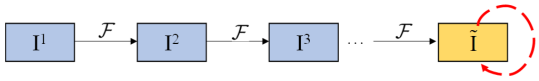

Fig. 2. The chain of repeated manipulations, where $\mathcal{F}$ denotes the specific manipulation and $\widetilde{I}$ is the convergent state.

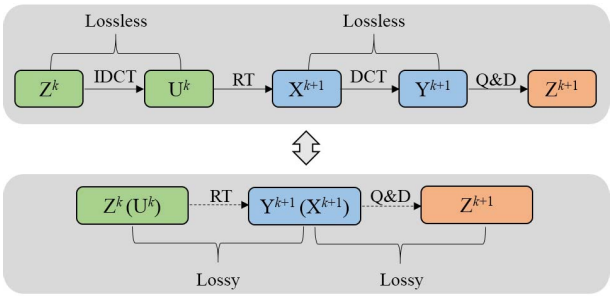

Fig. 3. The chain of Z^k in successive JPEG compressions.

Moreover, we define the quantization error block as

$$E^k = Y^k - Z^k. \tag{6}$$

The above defined blocks will be analyzed in the following context for a theoretical basis of the proposed method.

Clearly, by these notations, Z^1 and Z^2 respectively denote the de-quantized JPEG coefficients in single and double JPEG compressions. Therefore, for a given JPEG image to be detected, after entropy decoding, the double JPEG compression detection task can be viewed as identifying Z^2 from Z^1.

B. Motivation

As known, in some forensic scenarios, if the same manipulation is repeatedly performed on an image, the resulting image sequence tends to be convergent. For a better illustration, Fig. 2 shows the chain of the repeated manipulations, where I^1 is a given image, $\mathcal{F}$ denotes a specific manipulation, and I^{k+1} is the derived image after applying the manipulation $\mathcal{F}$ for k times. With these notations, the sequence $\{I^k\}_{k\geq 1}$ converges to an image denoted $\widetilde{I}$. However, the original image I^1 and its manipulated version $I^2 = \mathcal{F}(I^1)$ have different convergent rates. Roughly speaking, there exists a function d such that $d(I^1, \widetilde{I})$ and $d(I^2, \widetilde{I})$ are rather different, where $d(I, \hat{I})$ measures a specifically defined difference between two images I and $\hat{I}$. Then, based on the measurement function d, the image manipulation $\mathcal{F}$ can be effectively detected. This convergent tendency has been widely used for audio, image and video forensics [9], [44]–[48].

Inspired by the aforementioned convergent phenomenon, we propose to investigate the property for the sequence $\{Z^k\}_{k\geq 1}$ in successive JPEG compressions, and then design statistical features for our detection task. As shown in the upper figure of Fig. 3, the successive JPEG compressions are summarized to the manipulation chain between Z^k and Z^{k+1}. Since IDCT and DCT are lossless, the chain can be simplified as $Z^k \to Y^{k+1} \to Z^{k+1}$ as shown in the lower figure of Fig. 3. Then, we will study the relationship between Z^k and Z^{k+1} in this chain. The key issue is to impose the following quantity called BQE, which is the difference between DCT coefficients Y^{k+1} and the de-quantized JPEG coefficients Z^k

$$W^k = Y^{k+1} - Z^k. \tag{7}$$

Then, the relationship between Z^{k+1} and Z^k is given by

$$Z^{k+1} = \left[\frac{Y^{k+1}}{Q}\right]Q = \left[\frac{W^k + Z^k}{Q}\right]Q = Z^k + \left[\frac{W^k}{Q}\right]Q. \tag{8}$$

Notice that, for a given k, if $[W^k/Q] = 0$, we have $Z^{k+1} = Z^k$. Then, according to (5), we can derive that $Y^{k+1} = Y^{k+2}$, and thus $W^{k+1} = W^k$. It implicates that Y^k, Z^k and W^k remain unchanged in the following recompressions, i.e., it is easy to prove that, by induction, $Y^{k+n} = Y^k$, $Z^{k+n} = Z^k$ and $W^{k+n} = W^k$ hold for any $n \geq 1$. In such scenario, W^k is called the stable BQE (SBQE). If $[W^k/Q] \neq 0$, considering the rounding and truncation errors, BQE can be classified into two categories, i.e., rounding error BQE (RBQE) and truncation error BQE (TBQE). As a result, given a singly compressed image, there are three types of BQEs which are listed as follows

$$\begin{cases} \text{SBQE}, & [W^1/Q] = 0 \\ \text{RBQE}, & [W^1/Q] \neq 0, X^2 = [U^1] \\ \text{TBQE}. & [W^1/Q] \neq 0, X^2 \neq [U^1] \end{cases}. \tag{9}$$

Since SBQE remains unchanged in the following recompressions, it is neither changed to RBQE nor TBQE. Furthermore, we find that RBQE and TBQE cannot be changed to each other, only to SBQE. In summary, after recompression, the state transition of the three types of BQEs is shown in Fig. 4. To illustrate this, we test BQE on 1,338 gray-scale images compressed with QF = 90 taken from UCID database [49]. The average numbers of the three types of BQEs are listed in Table I. We can see that the number of SBQE increases while that of RBQE and TBQE decreases with recompression. Moreover, the change speed of RBQE is faster than that of TBQE. For a better demonstration, the state transitions of the three types of BQEs in successive compressed images are shown Fig. 5. As can be seen, RBQE and TBQE are changed to SBQE after recompression. Based on the above analysis, two facts can be observed: i) both RBQE and TBQE converge to SBQE after repeated recompressions, ii) SBQE is

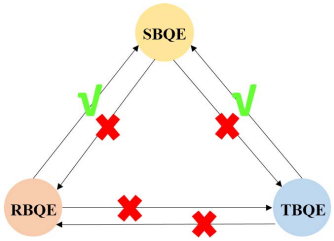

Fig. 4. State transition of the three types of BQEs.

TABLE I
THE AVERAGE NUMBERS OF THREE TYPES OF BQES ON UCID WITH QF=90

	$k=1$	$k=3$	$k=5$	$k=7$	$k=11$
SBQE	2919	3040	3063	3070	3072
RBQE	82	0	0	0	0
TBQE	71	32	9	2	0

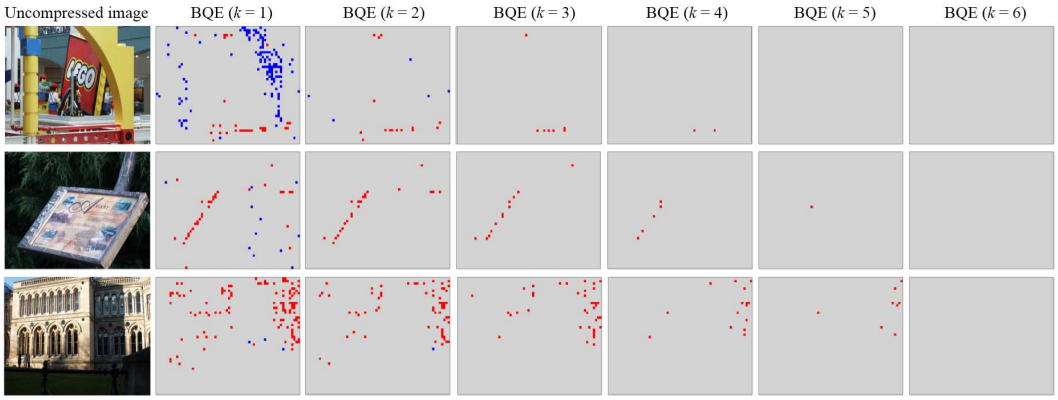

Fig. 5. Variation of BQE: SBQE, RBQE and TBQE blocks are marked in gray, blue and red, respectively.

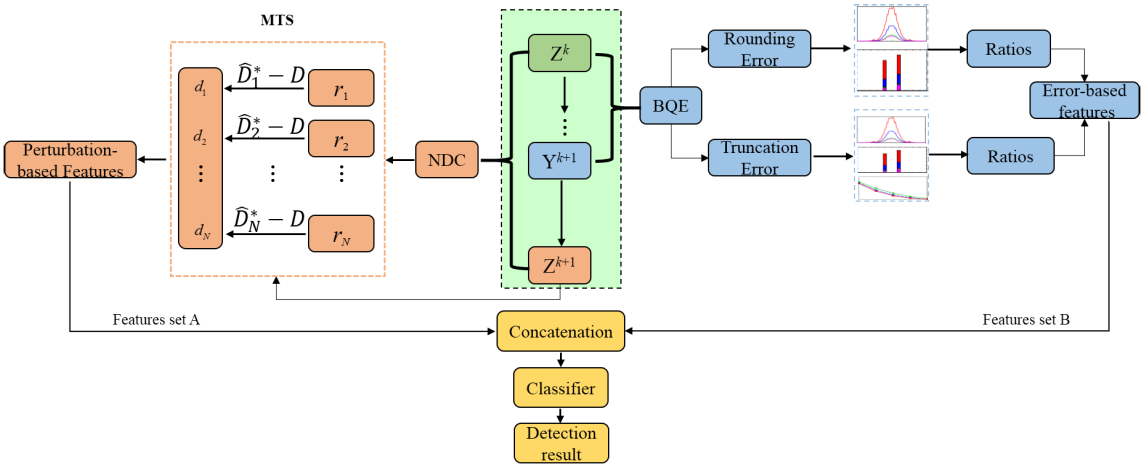

Fig. 6. The flowchart of the proposed method for double JPEG compression detection.

useless for the detection. As a consequence, the convergent rate of RBQE/TBQE can be employed as a clue for the detection.

Regarding (7), from the perspective of the difference between Y^{k+1} and Z^k, BQE only reflects partial information for the sequence $\{Z^k\}_{k\geq 1}$. However, it cannot completely capture the variation tendency of such sequence. Then, NDC is considered as the other investigation of such tendency from the view of JPEG coefficients. According to (8), the monotone decreasing of NDC in successive recompressions, observed in [38] and our previous work [40], can be theoretically explained. As a result, the convergent rate of NDC for double compression is faster than that for single compression. In summary, the convergent rates of BQE and NDC for single and double compressions are different, which are considered as the clues for detecting double JPEG compression with the same quantization matrix.

III. Proposed Method

In this section, by leveraging the convergence property of rounding/truncation errors and JPEG coefficients, a novel method for double JPEG compression detection is proposed. The flowchart of the proposed method is shown in Fig. 6 for clarity. Firstly, BQE is analyzed and a set of ratios for non-zero RBQE/TBQE (error-based features) is respectively extracted to characterize the convergent tendency of rounding/truncation errors. Then, considering NDC, a new perturbation strategy is presented, in which multiple thresholds are exploited with different modification ratios on JPEG coefficients, and the differences between the multiple thresholds and NDC (perturbation-based features) are utilized as features for measuring the convergent property of JPEG coefficients. Finally, the extracted features are concatenated into a 15-D vector and then fed into SVM for the detection.

A. Analysis on BQE and the Error-Based Features

For SBQE, we know that $W^{k+1} = W^k$ holds for each $k \geq 1$, thus it cannot provide discriminative information for distinguishing double compression from single compression. As a result, SBQE is excluded for the detection. We then study the relationship between W^{k+1} and W^k for RBQE and TBQE, respectively.

1) RBQE: Clearly, we can prove that

$$W^{k+1} = \mathrm{DCT}\left(\left\{\mathrm{IDCT}\left(W^k - \left[\frac{W^k}{Q}\right]Q\right)\right\}\right), \tag{10}$$

where $\{x\} = x - [x]$ means the decimal part of x. The proof of (10) can be found in Appendix.

First, consider a simple case that $Q = \mathbf{1}$ which is the matrix with each element q_i equals 1, i.e., QF = 100, the above

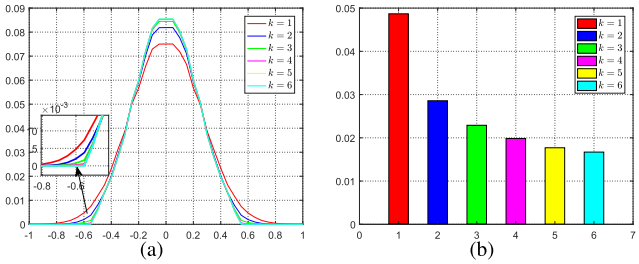

Fig. 7. RBQE: (a) the average distribution and (b) the corresponding average RQR for QF=100 on UCID.

equation (10) can be then rewritten as

$$W^{k+1} = \mathrm{DCT}(\{\mathrm{IDCT}(\{W^k\})\}). \tag{11}$$

As DCT/IDCT is an orthogonal transform and

$$\{x\}^2 \le x^2 + \min(0, 1 - 2|x|) \le x^2 \tag{12}$$

holds for each $x \in \mathbb{R}$, we have

$$\begin{aligned} \|W^{k+1}\|^2 &= \|\{\mathrm{IDCT}(\{W^k\})\}\|^2 \\ &\le \|\mathrm{IDCT}(\{W^k\})\}\|^2 \\ &= \|\{W^k\}\|^2 \\ &\le \|W^k\|^2 + \sum_{i=0}^{63} \min(0, 1 - 2|W_i^k|) \end{aligned} \tag{13}$$

and thus

$$\|W^{k+1}\| \le \|W^k\| \tag{14}$$

where $\|\cdot\|$ denotes the usual l_2-norm, and $(W_0^k, \ldots, W_{63}^k)$ is the vector form of W^k. Based on (13), for any $\varepsilon > 0$, we know that there is only finite (k, i) satisfying $|W_i^k| \ge \frac{1}{2} + \varepsilon$. Otherwise, $\|W^k\| \to -\infty$ when $k \to +\infty$, which is a contradiction. This indicates that, for each i

$$\overline{\lim_{k\to\infty}} |W_i^k| \le \frac{1}{2} + \varepsilon. \tag{15}$$

As ε is arbitrary, we then have

$$\overline{\lim_{k\to\infty}} |W_i^k| \le \frac{1}{2} \tag{16}$$

which says that

$$\overline{\lim_{k\to\infty}} \|W^k\|_\infty \le \frac{1}{2}. \tag{17}$$

Based on (14)–(17), we know that after multiple recompressions, the l_2-norm of W^k decreases and thus converges. Moreover, the maximum of $|W_i^k|$ approximates to 1/2. Fig. 7(a) shows the average distribution of RBQE on UCID database with QF $= 100$ for k times ($1 \le k \le 6$) compressions. It is clear that i) the distribution tends to become convergent, ii) the maximum and minimum of RBQE respectively approximate to $\frac{1}{2}$ and $-\frac{1}{2}$ for increasing k, iii) the distribution with the $(k+1)$-th compression is closer to the convergent state than that with the k-th compression. Thus, the distance between the distribution for single compression and the convergent state is larger than that for double compression. To measure such distance, the ratio of non-zero quantized RBQE (RQR), i.e., the ratio of RBQE outside $[-\frac{q_i}{2}, \frac{q_i}{2}]$, is considered as a simple metric. Fig. 7(b) shows the average RQR on UCID with QF $= 100$. Clearly, RQR decreases and tends to converge with k increasing. Importantly, for single compression ($k = 1$), RQR is larger than that for double compression ($k = 2$). Consequently, RQR is utilized as one feature for detection.

When $Q \ne \mathbf{1}$, i.e., QF $\ne 100$, it is hard to provide theoretical analysis of the relationship between W^{k+1} and W^k. We experimentally analyze RBQE in successive recompressions. Fig. 8 shows the average RQR with QF $= 95, 90, 85$ for k times compressions. It is observed that RQR tends to be stable after multiple recompressions. Obviously, RQR for single compression is larger than that for double compression, especially for QF ≤ 90. For example, RQR of single compression is 0.014 while it almost changes to zero after double compression when QF $= 85$. Moreover, the average distributions of RBQE are also reported in Fig. 9(a)–(c). It can be seen that the distribution gradually shrinks toward the center. To measure the variation tendency of such distribution, the ratio of non-zero RBQE (RR), i.e., the area under the distribution, is considered as the other metric. The corresponding average RR is shown in Fig. 9(d), where RR for single compression is larger than that for double compression. Especially for QF ≤ 90, RR almost tends to zero after double compression. Thus, RR also can be utilized for detection.

In summary, two features, i.e., RQR and RR, are proposed from RBQE for double JPEG compression detection.

2) TBQE: Since there is a lack of theoretical model for truncation error, in the following context, we experimentally discuss the convergence of TBQE.

Firstly, the ratios of non-zero quantized TBQE (RQT) with QF $= 100, 95, 90$ are shown in Fig. 10. As can be seen that RQT decreases with k increasing. That is, for single compression, RQT is larger than that for double compression. Then, the distributions of TBQE with QF $= 100, 95, 90$ are also shown in Fig. 11(a)–(c). It is observed that the distribution of TBQE for the $(k+1)$-th compression is always lower than that for the k-th compression. As a result, the ratio of non-zero TBQE (RT) for the k-th compression is larger than that for the $(k+1)$-th compression (see Fig. 11(d)).

An interesting observation is that the average ratio of the number of TBQE to the number of truncation error blocks, called RTT, tends to converge after multiple recompressions. Fig. 12 shows the variation tendency of the average RTT with different QFs for k times compressions. It can be seen that RTT of single compression is larger than that of double compression, then it tends to be stable when $k = 6$. Based on the above analysis, three features, i.e., RQT, RT and RTT, are proposed from TBQE for our detection task.

In summary, such ratios, i.e., RR, RT, RQR, RQT and RTT, are computed as the error-based features to measure the convergent rates of RBQE and TBQE for double compression detection.

B. Analysis on JPEG Coefficients and the Perturbation-Based Features

The error-based features only partially exploit $\{Z^k\}_{k\ge1}$. However, they cannot completely capture the variation

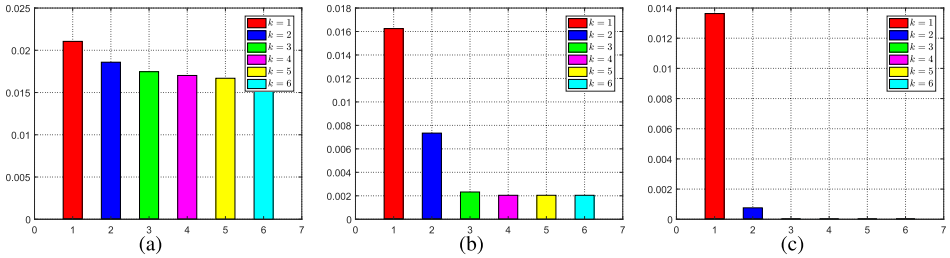

Fig. 8. The average RQR for (a) QF=95, (b) QF=90 and (c) QF=85.

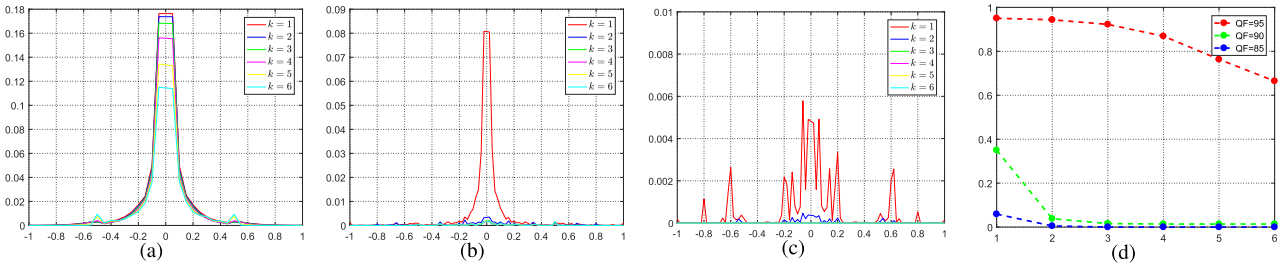

Fig. 9. The average distribution of RBQE for (a) QF=95, (b) QF=90, (c) QF=85 and (d) the corresponding average RR.

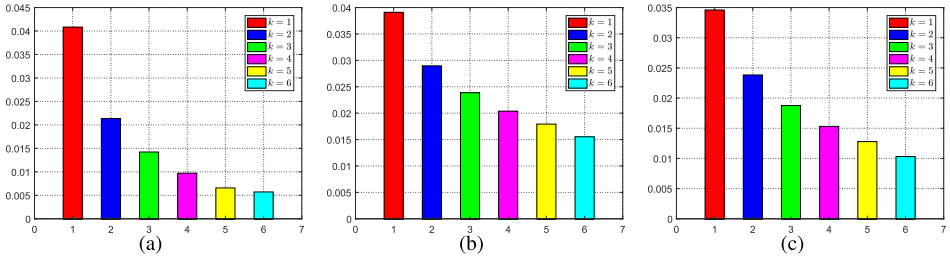

Fig. 10. The average RQT for (a) QF=100, (b) QF=95 and (c) QF=90.

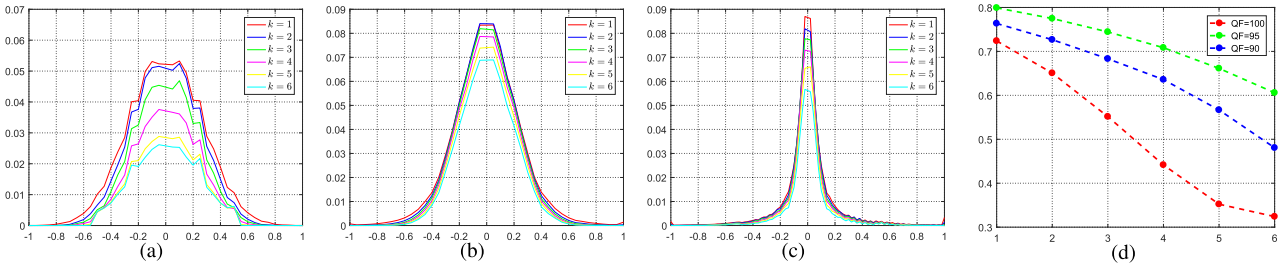

Fig. 11. The average distribution of TBQE for (a) QF=100, (b) QF=95, (c) QF=90, and (d) the corresponding average RT.

tendency of such sequence. In this subsection, from the view of JPEG coefficients, NDC is exploited to investigate $\{Z^k\}_{k\geq 1}$. First, an analysis of the perturbation strategy on JPEG coefficients is provided and then MTS is proposed by exploring multiple thresholds. Finally, the differences between the multiple thresholds and NDC are utilized as the perturbation-based features for the detection.

In [38] and our previous work [40], for a given JPEG image to be detected, the single threshold based random perturbation strategy is adopted to find a proper ratio for JPEG coefficients modification and then obtain an image dependent threshold $\widehat{D}$. By comparing $\widehat{D}$ with the NDC denoted as D, double JPEG compression can be distinguished as follows

$$\begin{cases} \text{double compression}, & \text{if } \widehat{D} \geq D \\ \text{single compression}, & \text{if } \widehat{D} < D \end{cases}. \tag{18}$$

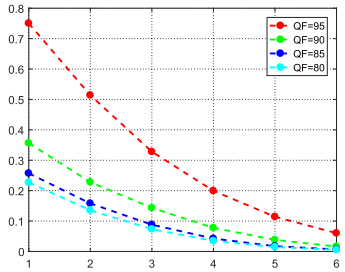

Fig. 12. Variation tendency of the average RTT for the k-th compression.

Recall here that, NDC is the number of different JPEG coefficients between the to be detected JPEG image and its recompressed version. Specifically, assume that B is a JPEG coefficients block in the JPEG image. It is modified by the perturbation strategy, then the modified version of B

is given by

$$B^*_{u,v} = B_{u,v} + \alpha_{u,v} \tag{19}$$

where $0 \leq u, v \leq 7$ is the selected frequency position, and $\alpha_{u,v} \in \{1, -1\}$ is the perturbation quantity, which is randomly determined.

We now analyze the perturbation strategy. For clarity, we consider a simple case that only one non-zero element is modified. The de-quantization and IDCT operations are applied on B^* in turn, then we have, by a simple deduction

$$C^*_{x,y} = C_{x,y} + \alpha c_{\hat{u}} c_{\hat{v}} Q_{\hat{u},\hat{v}} \cos\frac{\hat{u}\pi(2x+1)}{16} \cos\frac{\hat{v}\pi(2y+1)}{16} \tag{20}$$

where $(\hat{u}, \hat{v})$ refers to the specific position of the modified JPEG coefficient in the 8×8 block, $c_t = \sqrt{1/8}$ if $t = 0$, $c_t = 1/2$ if $t \neq 0$, C and C^* are the results by performing IDCT on B and B^*, respectively. Then the absolute difference between $C_{x,y}$ and $C^*_{x,y}$ is

$$\triangle_{x,y} = c_{\hat{u}} c_{\hat{v}} Q_{\hat{u},\hat{v}} \left| \cos\frac{\hat{u}\pi(2x+1)}{16} \cos\frac{\hat{v}\pi(2y+1)}{16} \right|. \tag{21}$$

According to (21), $\triangle_{x,y}$ only depends on the quantization step $Q_{\hat{u},\hat{v}}$. If $Q_{\hat{u},\hat{v}}$ is a large quantization step, the difference $\triangle_{x,y}$ is large as well and thus the block C is severely perturbed. That is, the range of rounding/truncation errors is going to be wide thus $\widehat{D}$ should be large based on (20). Since the quantization steps are different with different frequency positions, the threshold $\widehat{D}$ is quite different for each modification. As a result, singly JPEG compressed images may be identified as doubly JPEG compressed ones even using the same modification ratio r. As a consequence, the main problem of single threshold based methods [38], [40] is that, on one hand, the modification ratio r is chosen from the entire database, which is not the optimal one for each individual image. On the other hand, the perturbation strategy has randomness and uncertainty, that leads to unstable detection results. To address these problems, MTS is proposed to extract the perturbation-based features. More specifically, given a to be detected JPEG image, the JPEG coefficients are randomly modified with different modification ratios r_n to obtain the multiple thresholds $\widehat{D}_n$. Here, $1 \leq n \leq N$ and $r_1 < r_2 < \ldots < r_N$. Then the differences between $\widehat{D}_n$ and D are explored for the perturbation-based features extraction. The benefits of MTS are summarised as follow. The set of r_n contains the optimal modification ratio for each individual image to the maximum extent, which deduces the misclassification probability. Moreover, the single threshold strategy can be considered as an individual classifier, which has different detection results with different thresholds. Due to the diversity of multiple thresholds, MTS is regarded as diverse individual learners that is able to achieve more stable and higher detection accuracies than those of the single threshold based strategy. The details of MTS are described in Section III-C.2.

C. Features Extraction

In this subsection, we introduce the features extraction procedure.

1) Error-Based Features Extraction: The error-based features, i.e., RR, RT, RQR, RQT, RTT, are extracted from RBQE and TBQE, respectively. More specifically, RR and RT are computed as follows

$$\begin{aligned} RR &= \int_{-\infty}^{-\theta} f_r(x)dx + \int_{\theta}^{\infty} f_r(x)dx \\ RT &= \int_{-\infty}^{-\theta} f_t(x)dx + \int_{\theta}^{\infty} f_t(x)dx \end{aligned} \tag{22}$$

where f_r and f_t are the distributions of RBQE and TBQE, respectively, and θ is set to 0.01. The ratios of non-zero quantized RBQE and TBQE, i.e., RQR and RQT, are calculated by

$$\begin{aligned} RQR &= \frac{\sum_{l=1}^{L_r} \sum_{u,v=0}^{7} \delta(S_{r,l}(u,v))}{64 L_r} \\ RQT &= \frac{\sum_{l=1}^{L_t} \sum_{u,v=0}^{7} \delta(S_{t,l}(u,v))}{64 L_t} \end{aligned} \tag{23}$$

where L_r and L_t are the numbers of RBQE and TBQE blocks, $S_{r,l}$ and $S_{t,l}$ denote the l-th quantized RBQE and TBQE, and $\delta(\cdot)$ is the indicator function defined as

$$\delta(x) = \begin{cases} 1, & \text{if } x \neq 0 \\ 0, & \text{if } x = 0. \end{cases} \tag{24}$$

Moreover, RTT is computed as the ratio of the number of TBQE blocks to the number of truncation error blocks. Eventually, the set of error-based features, E_fea, is

$$\text{E\_fea} = \{RR, RT, RQR, RQT, RTT\}. \tag{25}$$

2) Perturbation-Based Features Extraction: Perturbation-based features are extracted based on MTS. The features extraction process is summarised as follows: Step 1)

1) Decompress the to be detected JPEG image J, and then compress it again with the same quantization matrix Q to obtain a new JPEG image K. The NDC between J and K is denoted as D.
2) Decode K to derive its JPEG coefficients and then randomly modify it with the modification ratio r_1 by the modification strategy. Then, encode the modified coefficients to generate a JPEG image K^*.
3) Decompress K^* into the spatial domain, and then recompress it with Q to obtain $\widehat{K}^*$. The NDC between K^* and $\widehat{K}^*$ is denoted as $\widehat{D}^*_1$.
4) Repeat the above two steps for $(N-1)$ times with different ratios $r_2, \ldots, r_N$ to derive the $(N-1)$ thresholds $\widehat{D}^*_2, \ldots, \widehat{D}^*_N$.
5) After the above procedures, the set of perturbation-based features is defined as P_fea $= \{d_1, \ldots, d_N\}$, where $d_n =$

TABLE II
DETECTION ACCURACY RATES (%) OF E_FEA, P_FEA AND EP_FEA ON THREE DATABASES

QF	UCID			BOSSbase			SYSU		
	E_fea	P_fea	EP_fea	E_fea	P_fea	EP_fea	E_fea	P_fea	EP_fea
95	100.00	100.00	100.00	99.99	100.00	100.00	99.99	100.00	100.00
90	98.57	96.67	99.52	98.01	98.27	99.20	99.36	96.06	99.78
85	94.30	94.31	95.67	95.05	95.06	98.02	76.04	82.08	82.70
80	95.44	93.22	96.11	95.06	93.14	98.32	80.30	84.41	85.53
75	82.15	83.80	84.76	74.88	79.31	86.36	69.12	78.27	79.15
70	79.02	82.23	82.34	70.29	78.61	84.55	70.13	74.91	76.01

TABLE III
TPR AND TNR OF THE PROPOSED METHOD ON THREE DATABASES

QF	UCID		BOSSbase		SYSU	
	TPR	TNR	TPR	TNR	TPR	TNR
95	100.00	100.00	100.00	100.00	100.00	100.00
90	99.53	99.50	99.17	99.23	99.80	99.76
85	95.46	95.88	98.28	97.76	84.73	80.65
80	96.04	96.19	98.33	98.32	85.56	85.50
75	83.85	85.66	86.67	86.06	78.77	79.52
70	82.31	82.36	85.05	84.06	73.84	78.19

$\text{sign}(\widehat{D}_n^* - D)$, with

$$\text{sign}(x) = \begin{cases} 1, & \text{if } x \geq 0 \\ 0, & \text{if } x < 0. \end{cases} \tag{26}$$

Finally, the features extracted from RBQE/TBQE as well as NDC are concatenated into a 15-D feature vector EP_fea = [E_fea, P_fea], then it is fed into SVM for double JPEG compression detection.

IV. EXPERIMENTAL RESULTS

A. Experimental Setup

1) Dataset: For the experiments, we build singly and doubly JPEG compressed images with raw images taken from UCID [49], BOSSbase [50] and SYSU [38] databases, respectively. UCID database consists of 1,338 images sized of 384×512 or 512×384. We randomly select 1,000 images from BOSSbase database with the size of 512×512. SYSU database contains 1,128 images sized of 512×512. All these images are first singly compressed to generate the negative samples.[1] The positive samples are obtained by recompressing those singly compressed images with the same quantization matrix.

2) Evaluation Criterion: We evaluate the proposed method in terms of true positive rate (TPR), true negative rate (TNR), and detection accuracy rate,[2] computed as $(\text{TPR} + \text{TNR})/2$. TPR (TNR) represents the proportion of correctly predicted doubly (singly) compressed images.

3) Parameter Set: For methods in [38] and [40], the proper ratios for JPEG coefficients modification are determined through exhaustive search. To extract the proposed P_fea, the number of different modification ratios is set to $N = 10$. Specifically, the modified ratios r_n are selected from the range of $[0.030, 0.048]$ with the step of 0.002. The soft-margin SVM with the Gaussian kernel is adopted and 20-fold grid searching is used to select parameters c and γ for the classifier. Half of the singly and doubly compressed images are randomly selected for training, and the remaining ones are used for testing. Each testing procedure is repeated over 20 times and the average detection accuracy rate is reported.

[1]The color images should be firstly converted into grayscale.

[2]The numbers of singly and doubly compressed images are equal in our experiments.

B. Evaluation of Different Subsets of Features

In this subsection, we first evaluate the performance of the proposed feature sets, i.e., E_fea, P_fea as well as the concatenated features EP_fea, for ablation study. The detection accuracy rates of the aforementioned three feature sets are listed in Table II. It is observed that E_fea outperforms P_fea with high QFs. For example, the detection accuracy rate of E_fea is 99.36%, which is higher than that (96.06%) of P_fea when QF = 90 on SYSU database. In addition, P_fea is more efficient than E_fea with low QFs. Compared with the two individual feature sets, the concatenated EP_fea can improve the detection performance to a higher level. It indicates that each individual subset of features can provide complementary discriminative information for double JPEG compression detection.

We also evaluate the proposed method with the criterions of TPR and TNR, as shown in Table III. We can observe that the TPRs and TNRs are considerably balanced in most cases while there exists a little unbalanced results for low QFs (See QF = 70 on SYSU). This can be explained that, in such scenario, the numbers of both RBQE and TBQE are quite small thus there is less useful information for feature extraction. Consequently, the features extracted from singly and doubly compressed images are indistinguishable, which results in biased detection results. Furthermore, TPRs and TNRs of methods [38], [40] based on single threshold are usually biased towards doubly JPEG compressed images with low QFs (see Tables 2 and 3 in [40]). The results in Tables II and III indicate the superiority of the proposed method both in accuracy and unbiasedness. Notice that, both TPR and TNR become worse with QF decreasing. The reason is that less discriminative information can be extracted from BQE with low QFs. We observe that if there is no RBQE

TABLE IV
DETECTION ACCURACY RATES (%) OF [38]–[40], AND THE PROPOSED METHOD ON THREE DATABASES

QF	UCID				BOSSbase				SYSU			
	[38]	[39]	[40]	Proposed	[38]	[39]	[40]	Proposed	[38]	[39]	[40]	Proposed
95	99.14	100.00	100.00	**100.00**	98.30	100.00	100.00	**100.00**	100.00	100.00	100.00	**100.00**
90	92.12	98.63	96.04	**99.52**	91.10	98.74	97.60	**99.20**	92.69	99.46	93.71	**99.78**
85	87.52	95.57	92.94	**95.67**	86.35	96.82	93.80	**98.02**	75.66	80.99	79.43	**82.70**
80	85.76	95.73	92.38	**96.11**	84.35	95.78	92.65	**98.32**	76.86	84.52	83.29	**85.53**
75	74.93	84.02	83.11	**84.76**	67.70	75.02	78.45	**86.36**	69.28	77.66	76.29	**79.15**
70	73.65	80.83	81.53	**82.34**	66.35	72.86	76.36	**84.55**	66.49	67.64	73.58	**76.01**
60	74.40	77.78	80.79	**82.18**	65.70	68.69	74.85	**81.01**	65.56	67.99	71.41	**73.08**
40	74.23	77.10	80.64	**81.12**	66.20	68.67	72.75	**78.47**	64.72	67.73	70.43	**71.47**

TABLE V
CROSS DETECTION ACCURACY RATES (%) OF THE PROPOSED METHOD AND [39] ON THREE DATABASES

QF	Training samples from UCID				Training samples from BOSSbase				Training samples from SYSU			
	Test on BOSSbase		Test on SYSU		Test on UCID		Test on SYSU		Test on UCID		Test on BOSSbase	
	[39]	Proposed	[39]	Proposed	[39]	Proposed	[39]	Proposed	[39]	Proposed	[39]	Proposed
95	**100.00**	99.10	100.00	**100.00**	99.73	**99.96**	**100.00**	99.52	**100.00**	99.85	**100.00**	99.90
90	97.25	**98.75**	96.89	**99.03**	99.15	**99.43**	97.97	**99.42**	89.83	**98.46**	85.60	**96.85**
85	96.15	**96.85**	78.59	**83.46**	71.11	**95.55**	70.47	**83.20**	93.27	**94.88**	91.35	**96.35**
80	96.30	**96.33**	75.84	**86.34**	81.20	**96.23**	67.95	**86.17**	92.15	**94.43**	93.16	**94.50**
75	70.10	**84.65**	79.29	**80.40**	58.89	**80.23**	62.01	**78.63**	83.81	**83.85**	74.20	**82.25**
70	**78.55**	77.08	64.76	**82.85**	60.50	**78.66**	60.29	**76.27**	**84.30**	78.88	77.50	**77.75**

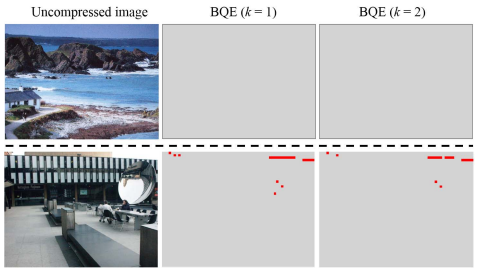

Fig. 13. Two failed examples with QF = 70 on UCID.

and TBQE in the first compression cycle, singly compressed image will be incorrectly identified as doubly compressed one in general. This is the case with the upper example in Fig. 13 where no useful information can be used for features extraction. Furthermore, the doubly compressed image is easily misclassified as the singly compressed one when there is slight difference between BQEs in the first two compression cycles. This is the case with the lower example in Fig. 13 where BQE does not change too much after recompression.

C. Comparison With Some State-of-the-Art Methods

In this subsection, the proposed method is compared with some state-of-the-art methods [38]–[40]. Detection accuracy rates of the four methods on the three databases are reported in Table IV. One can observe that the proposed method is superior to the other three methods with various QFs and databases. Especially on BOSSbase database with QF = 70, the proposed method can achieve the detection accuracy rate of 84.55%, which is 18%, 12%, and 8% higher than those of [38]–[40], respectively. Furthermore, compared with the results in Table II, we can see that the proposed features set P_fea is able to achieve higher accuracies than those of [40] in all tested QFs. For example, when QF = 85, P_fea achieves the detection accuracy rates of 94.31%, 95.06% and 82.08% on UCID, BOSSbase and SYSU databases, respectively. However, in the same setting, the method [40] based on single threshold strategy yields accuracies of 92.94%, 93.80% and 79.43%. It also demonstrates that MTS is more discriminative than the single threshold based strategy for the detection.

D. Cross Detection Results

To verify the universality of the proposed method, we also implement the cross detection experiment. That is, the SVM trained from one of the three databases classifies images from the other two. The detection accuracy rates are reported in Table V. The proposed method achieves superior detection performance to [39] in most cases, indicating that, in general, the proposed method has better generalization ability than [39] for mismatched databases. Compared with Table IV, the general accuracy rates of the proposed method and [39] decrease to some content, which is due to the mismatched statistical differences between training and testing samples. However, there are some unexpected results. For example, when both training and testing on UCID at QF = 70, the accuracy rate of [39] is 80.83%, which is lower than that (84.30%) of training on SYSU. For the proposed method, when both training and testing on SYSU at QF = 75, the accuracy rate is 79.15%, which is lower than that (80.40%) of training on UCID. The presence of such unexpected results can be explained as follows. Clearly, if there exists considerable statistical differences between training and testing samples, then a SVM classifier unbiased for the training samples may produce a biased detection result for the testing samples. Furthermore, the balance between TPR and TNR is usually achieved at the expense of accuracy. That is, an unbiased SVM classifier is probably not the one that achieves the highest accuracy. As a result, an unbiased SVM classifier trained on

TABLE VI
COMPARISON RESULTS (%) OF TRIPLE JPEG COMPRESSION DETECTION ON UCID DATABASE

QF	Single-Triple				Double-Triple			
	[38]	[39]	[40]	Proposed	[38]	[39]	[40]	Proposed
95	100.00	100.00	100.00	**100.00**	99.03	99.88	99.40	**99.89**
90	96.26	99.75	98.51	**99.82**	67.85	80.49	67.68	**84.37**
85	92.89	96.91	96.97	**97.71**	67.12	72.62	68.87	**80.31**
80	91.59	96.79	96.11	**97.32**	66.70	70.68	69.81	**82.36**
75	82.84	86.51	88.94	**90.26**	67.75	70.49	72.05	**80.69**
70	81.39	84.05	87.11	**88.48**	67.08	68.60	72.83	**82.13**

TABLE VII
DETECTION ACCURACY RATES (%) ON SMALL PATCHES WITH SIZES OF 256×256 AND 128×128 ON UCID DATABASE

QF	256×256				128×128			
	[38]	[39]	[40]	Proposed	[38]	[39]	[40]	Proposed
95	98.73	**99.98**	99.81	99.86	98.28	**99.98**	99.40	99.70
90	86.43	95.34	89.29	**97.91**	74.74	76.05	74.96	**82.72**
85	80.64	85.72	83.26	**86.99**	66.26	66.63	68.80	**70.74**
80	78.06	85.22	82.88	**86.10**	65.32	65.48	67.83	**68.67**
75	70.25	71.90	73.58	**75.59**	59.64	59.90	63.30	**63.97**
70	70.03	72.43	73.54	**75.26**	61.03	61.35	63.34	**63.41**

an image database produces a biased detection result with a higher accuracy when it is tested on another database. As for the aforementioned example of [39], when training and testing both on UCID, the TPR and TNR are 80.82% and 80.84%, respectively, indicating the detection results are well balanced. In contrast, when training on SYSU and testing on UCID, although the classifier achieves a higher accuracy (84.30%) than that of the proposed method, but with an imbalance between TPR (90.43%) and TNR (78.17%).

E. Triple JPEG Compression Detection

In this subsection, further experiments are conducted on UCID database for detecting triple JPEG compression. The comparison results of Single-Triple and Double-Triple JPEG compression detections are listed in Table VI. It can be seen that the proposed method achieves the highest detection accuracy rates among the four methods in all tested QFs. For example, the detection accuracy rate of the proposed method is 82.13%, which is 15%, 11% and 9% higher than those of methods [38]–[40] for Double-Triple case when $QF = 70$, respectively. Clearly, the detection accuracy rates of Single-Triple JPEG compressions detection are higher than those of Double-Triple JPEG compressions. This comes from the fact that the statistical differences between single and triple JPEG compressions are larger than those between double and triple JPEG compressions.

F. Evaluation on Small Image Patches

Before ending the evaluation, we perform one more test to verify the performance of the proposed method on small image patches. When a portion of a raw image is copy-pasted into a JPEG image and then the forged image is compressed with the same quantization matrix used for the JPEG image. The ability to detect double JPEG compression on small patches is essential for tampering localization. The experiments are conducted on image patches with two different sizes, i.e., 256×256 and 128×128. These patches are central cropped from the full sized images on UCID database. Table VIII shows the detection accuracy rates of the proposed method and [38]–[40]. We can observe that the performance of the proposed method are superior to those of the best one in almost all scenarios, except for $QF = 95$. It implies that the proposed method has more practical applications than the state-of-the-art schemes.

TABLE VIII
DETECTION ACCURACY RATES (%) WITHOUT AND WITH MKL ON UCID DATABASE

QF	SVM	MKL-SVM
95	100.00	**100.00**
90	99.52	**99.55**
85	95.67	**99.81**
80	96.11	**96.56**
75	84.76	**86.55**
70	82.34	**84.01**
60	82.18	**82.81**
40	81.12	**82.66**

G. Classification Accuracy of MKL-SVM

Since classical SVM is a single kernel based learning algorithm, the detection accuracy rates of the proposed method for the detection task can be further improved by adopting the multiple kernels learning (MKL) [51]. Two Gaussian kernels and two polynomial kernels are exploited in the experiment. Table VIII shows the detection accuracy rates with MKL and we can observe that the improvement is obvious, especially for the case that QF is less than 80. For example, the detection performance is improved by 1.7% for $QF = 75$ with MKL. Besides, the improved accuracies are also higher than those of [38]–[40].

V. Conclusion

In this paper, a novel method is proposed to detect double JPEG compression with the same quantization matrix. Based on an in-depth analysis of the pipeline in successive JPEG compressions, we find that the rounding/truncation errors as well as JPEG coefficients tend to converge after multiple recompressions. Then, BQE is defined, and we derive that the ratio of non-zero BQE for single compression is larger than that for double compression. Base on this fact, error-based features are extracted from rounding and truncation error blocks, respectively. To leverage the convergence property of JPEG coefficients, MTS is designed, in which multiple thresholds are derived with different modification ratios on JPEG coefficients. Then, perturbation-based features are extracted from the differences between the multiple thresholds and NDC to be a supplementary. Finally, the error- and perturbation-based features are concatenated into a 15-D vector for the detection. Extensive experimental results demonstrate that the proposed method provides superior performance to some state-of-the-art works. In our future work, it is worth making a thorough analysis on the truncation error blocks, especially for low QFs. Additionally, the convergence of rounding/truncation errors and JPEG coefficients in higher JPEG compression cycles can be used to discriminate multiple compressions.

Appendix

According to (6)–(8), we have

$$E^{k+1} = Y^{k+1} - Z^{k+1} = W^k - \left[\frac{W^k}{Q}\right]Q. \tag{27}$$

To simplify the analysis, we define

$$e^k = X^k - U^k = \mathrm{IDCT}(Y^k - Z^k) = \mathrm{IDCT}(E^k). \tag{28}$$

Then, we can obtain that

$$\begin{aligned} W^k &= \mathrm{DCT}(\mathrm{IDCT}(Y^{k+1} - Z^k)) \\ &= \mathrm{DCT}(X^{k+1} - U^k) \\ &= \mathrm{DCT}([U^k] - U^k) \\ &= \mathrm{DCT}([X^k - e^k] - X^k + e^k) \\ &= \mathrm{DCT}(e^k - [e^k]) = \{e^k\} \\ &= \mathrm{DCT}(\{\mathrm{IDCT}(E^k)\}). \end{aligned} \tag{29}$$

Here, recall that $\{x\} = x - [x]$. Based on (27) and (29), the relationship between W^{k+1} and W^k can be established as

$$\begin{aligned} W^{k+1} &= \mathrm{DCT}(\{\mathrm{IDCT}(E^{k+1})\}) \\ &= \mathrm{DCT}\left(\left\{\mathrm{IDCT}\left(W^k - \left[\frac{W^k}{Q}\right]Q\right)\right\}\right). \end{aligned} \tag{30}$$

References

[1] H. Li, W. Luo, X. Qiu, and J. Huang, "Identification of various image operations using residual-based features," *IEEE Trans. Circuits Syst. Video Technol.*, vol. 28, no. 1, pp. 31–45, Jan. 2018.

[2] Y. Guo, X. Cao, W. Zhang, and R. Wang, "Fake colorized image detection," *IEEE Trans. Inf. Forensics Security*, vol. 13, no. 8, pp. 1932–1944, Aug. 2018.

[3] C.-T. Li and Y. Li, "Color-decoupled photo response non-uniformity for digital image forensics," *IEEE Trans. Circuits Syst. Video Technol.*, vol. 22, no. 2, pp. 260–271, Feb. 2012.

[4] J. Wang, T. Li, X. Luo, Y.-Q. Shi, and S. K. Jha, "Identifying computer generated images based on quaternion central moments in color quaternion wavelet domain," *IEEE Trans. Circuits Syst. Video Technol.*, vol. 29, no. 9, pp. 2775–2785, Sep. 2019.

[5] X. Zhao, S. Wang, S. Li, and J. Li, "Passive image-splicing detection by a 2-D noncausal Markov model," *IEEE Trans. Circuits Syst. Video Technol.*, vol. 25, no. 2, pp. 185–199, Feb. 2015.

[6] S. Chen, S. Tan, B. Li, and J. Huang, "Automatic detection of object-based forgery in advanced video," *IEEE Trans. Circuits Syst. Video Technol.*, vol. 26, no. 11, pp. 2138–2151, Nov. 2016.

[7] J.-M. Guo, Y.-F. Liu, and Z.-J. Wu, "Duplication forgery detection using improved DAISY descriptor," *Expert Syst. Appl.*, vol. 40, no. 2, pp. 707–714, 2013.

[8] C. Chen, J. Ni, and J. Huang, "Blind detection of median filtering in digital images: A difference domain based approach," *IEEE Trans. Image Process.*, vol. 22, no. 12, pp. 4699–4710, Dec. 2013.

[9] X. Kang, M. C. Stamm, A. Peng, and K. J. R. Liu, "Robust median filtering forensics using an autoregressive model," *IEEE Trans. Inf. Forensics Security*, vol. 8, no. 9, pp. 1456–1468, Sep. 2013.

[10] J. Chen, X. Kang, Y. Liu, and Z. J. Wang, "Median filtering forensics based on convolutional neural networks," *IEEE Signal Process. Lett.*, vol. 22, no. 11, pp. 1849–1853, Nov. 2015.

[11] Y. K. Niu, Y. Zhao, and R. Ni, "Robust median filtering detection based on local difference descriptor," *Signal Process., Image Commun.*, vol. 53, pp. 65–72, Apr. 2017.

[12] B. Mahdian and S. Saic, "Blind authentication using periodic properties of interpolation," *IEEE Trans. Inf. Forensics Security*, vol. 3, no. 3, pp. 529–538, Sep. 2008.

[13] J. Bunk *et al.*, "Detection and localization of image forgeries using resampling features and deep learning," in *Proc. IEEE Conf. Comput. Vis. Pattern Recognit. Workshops (CVPRW)*, Jul. 2017, pp. 1881–1889.

[14] X. Liu, W. Lu, Q. Zhang, J. Huang, and Y.-Q. Shi, "Downscaling factor estimation on pre-JPEG compressed images," *IEEE Trans. Circuits Syst. Video Technol.*, vol. 30, no. 3, pp. 618–631, Mar. 2020.

[15] F. Ding, H. Wu, G. Zhu, and Y.-Q. Shi, "METEOR: Measurable energy map toward the estimation of resampling rate via a convolutional neural network," *IEEE Trans. Circuits Syst. Video Technol.*, vol. 30, no. 12, pp. 4715–4727, Dec. 2020.

[16] G. Cao, Y. Zhao, R. Ni, and X. Li, "Contrast enhancement-based forensics in digital images," *IEEE Trans. Inf. Forensics Security*, vol. 9, no. 3, pp. 515–525, Mar. 2014.

[17] M. Stamm and K. J. R. Liu, "Blind forensics of contrast enhancement in digital images," in *Proc. 15th IEEE Int. Conf. Image Process.*, Oct. 2008, pp. 3112–3115.

[18] L. Wen, H. Qi, and S. Lyu, "Contrast enhancement estimation for digital image forensics," *ACM Trans. Multimedia Comput., Commun., Appl.*, vol. 14, no. 2, pp. 1–21, May 2018.

[19] E. Kee, M. K. Johnson, and H. Farid, "Digital image authentication from JPEG headers," *IEEE Trans. Inf. Forensics Security*, vol. 6, no. 3, pp. 1066–1075, Sep. 2011.

[20] W. Luo, J. Huang, and G. Qiu, "JPEG error analysis and its applications to digital image forensics," *IEEE Trans. Inf. Forensics Security*, vol. 5, no. 3, pp. 480–491, Sep. 2010.

[21] T. H. Thai, R. Cogranne, F. Retraint, and T.-N.-C. Doan, "JPEG quantization step estimation and its applications to digital image forensics," *IEEE Trans. Inf. Forensics Security*, vol. 12, no. 1, pp. 123–133, Jan. 2017.

[22] J. Yang, Y. Zhang, G. Zhu, and S. Kwong, "A clustering-based framework for improving the performance of JPEG quantization step estimation," *IEEE Trans. Circuits Syst. Video Technol.*, vol. 31, no. 4, pp. 1661–1672, Apr. 2021.

[23] T. Bianchi, A. De Rosa, and A. Piva, "Improved DCT coefficient analysis for forgery localization in JPEG images," in *Proc. IEEE Int. Conf. Acoust., Speech Signal Process. (ICASSP)*, May 2011, pp. 2444–2447.

[24] T. Bianchi and A. Piva, "Detection of nonaligned double JPEG compression based on integer periodicity maps," *IEEE Trans. Inf. Forensics Security*, vol. 7, no. 2, pp. 842–848, Apr. 2012.

[25] I. Amerini, R. Becarelli, R. Caldelli, and A. D. Mastio, "Splicing forgeries localization through the use of first digit features," in *Proc. IEEE Int. Workshop Inf. Forensics Secur. (WIFS)*, Dec. 2014, pp. 143–148.

[26] W. Wang, J. Dong, and T. Tan, "Exploring DCT coefficient quantization effects for local tampering detection," *IEEE Trans. Inf. Forensics Security*, vol. 9, no. 10, pp. 1653–1666, Oct. 2014.

[27] T. Pevny and J. Fridrich, "Detection of double-compression in JPEG images for applications in steganography," *IEEE Trans. Inf. Forensics Security*, vol. 3, no. 2, pp. 247–258, Jun. 2008.
[28] T. D. Denemark, M. Boroumand, and J. Fridrich, "Steganalysis features for content-adaptive JPEG steganography," *IEEE Trans. Inf. Forensics Security*, vol. 11, no. 8, pp. 1736–1746, Aug. 2016.
[29] J. Lukas and J. Fridrich, "Estimation of primary quantization matrix in double compressed JPEG images," in *Proc. Digit. Forensic Res. Workshop*, 2003, pp. 5–8.
[30] A. C. Popescu and H. Farid, "Statistical tools for digital forensics," in *Proc. 6th Int. Workshop Inf. Hiding*, 2004, pp. 128–147.
[31] D. Fu, Y. Q. Shi, and W. Su, "A generalized Benford's law for JPEG coefficients and its applications in image forensics," in *Proc. 15th Secur., Steganography, Watermarking Multimedia Contents*, Feb. 2007, 65051L.
[32] B. Li, Y. Q. Shi, and J. Huang, "Detecting doubly compressed JPEG images by using mode based first digit features," in *Proc. IEEE 10th Workshop Multimedia Signal Process.*, Oct. 2008, pp. 730–735.
[33] C. Chen, Y. Q. Shi, and W. Su, "A machine learning based scheme for double JPEG compression detection," in *Proc. 19th Int. Conf. Pattern Recognit.*, Dec. 2008, pp. 1–4.
[34] Q. Wang and R. Zhang, "Double JPEG compression forensics based on a convolutional neural network," *EURASIP J. Inf. Secur.*, vol. 2016, no. 1, pp. 1–12, Dec. 2016.
[35] M. Barni *et al.*, "Aligned and non-aligned double JPEG detection using convolutional neural networks," *J. Vis. Commun. Image Represent.*, vol. 49, pp. 153–163, Nov. 2017.
[36] I. Amerini, T. Uricchio, L. Ballan, and R. Caldelli, "Localization of JPEG double compression through multi-domain convolutional neural networks," in *Proc. IEEE Conf. Comput. Vis. Pattern Recognit. Workshops (CVPRW)*, Jul. 2017, pp. 1865–1871.
[37] J. Park, D. Cho, W. Ahn, and H.-K. Lee, "Double JPEG detection in mixed JPEG quality factors using deep convolutional neural network," in *Proc. Eur. Conf. Comput. Vis. (ECCV)*, 2018, pp. 636–652.
[38] F. Huang, J. Huang, and Y. Q. Shi, "Detecting double JPEG compression with the same quantization matrix," *IEEE Trans. Inf. Forensics Security*, vol. 5, no. 4, pp. 848–856, Dec. 2010.
[39] J. Yang, J. Xie, G. Zhu, S. Kwong, and Y.-Q. Shi, "An effective method for detecting double JPEG compression with the same quantization matrix," *IEEE Trans. Inf. Forensics Security*, vol. 9, no. 11, pp. 1933–1942, Nov. 2014.
[40] Y. Niu, X. Li, Y. Zhao, and R. Ni, "An enhanced approach for detecting double JPEG compression with the same quantization matrix," *Signal Process., Image Commun.*, vol. 76, pp. 89–96, Aug. 2019.
[41] X. Huang, S. Wang, and G. Liu, "Detecting double JPEG compression with same quantization matrix based on dense CNN feature," in *Proc. 25th IEEE Int. Conf. Image Process. (ICIP)*, Oct. 2018, pp. 3813–3817.
[42] P. Peng, T. Sun, X. Jiang, K. Xu, B. Li, and Y. Shi, "Detection of double JPEG compression with the same quantization matrix based on convolutional neural networks," in *Proc. Asia–Pacific Signal Inf. Process. Assoc. Annu. Summit Conf. (APSIPA ASC)*, Nov. 2018, pp. 717–721.
[43] A. N. Harish, V. Verma, and N. Khanna, "Double JPEG compression detection for distinguishable blocks in images compressed with same quantization matrix," in *Proc. IEEE 30th Int. Workshop Mach. Learn. Signal Process. (MLSP)*, Sep. 2020, pp. 1–6.
[44] S. Lai and R. Böhme, "Block convergence in repeated transform coding: JPEG-100 forensics, carbon dating, and tamper detection," in *Proc. IEEE Int. Conf. Acoust., Speech Signal Process.*, May 2013, pp. 3028–3032.
[45] X. Jiang, P. He, T. Sun, F. Xie, and S. Wang, "Detection of double compression with the same coding parameters based on quality degradation mechanism analysis," *IEEE Trans. Inf. Forensics Security*, vol. 13, no. 1, pp. 170–185, Jan. 2018.
[46] W. Li, R. Ni, X. Li, and Y. Zhao, "Robust median filtering detection based on the difference of frequency residuals," *Multimedia Tools Appl.*, vol. 78, no. 7, pp. 8363–8381, 2018.
[47] C. Pasquini, G. Boato, N. Alajlan, and F. G. B. De Natale, "A deterministic approach to detect median filtering in 1D data," *IEEE Trans. Inf. Forensics Security*, vol. 11, no. 7, pp. 1425–1437, Jul. 2016.
[48] B. Li, T.-T. Ng, X. Li, S. Tan, and J. Huang, "Revealing the trace of high-quality JPEG compression through quantization noise analysis," *IEEE Trans. Inf. Forensics Security*, vol. 10, no. 3, pp. 558–573, Mar. 2015.
[49] G. Schaefer and M. Stich, "UCID: An uncompressed color image database," in *Proc. SPIE*, Dec. 2003, pp. 472–480.
[50] P. Bas, T. Filler, and T. Pevný, "'Break our steganographic system': The ins and outs of organizing BOSS," in *Proc. 13th Int. Conf. Inf. Hiding.*, 2011, pp. 59–70.
[51] A. Rakotomamonjy, F. Bach, S. Canu, and Y. Grandvalet, "SimpleMKL," *J. Mach. Learn. Res.*, vol. 9, pp. 2491–2521, Nov. 2008.

Yakun Niu received the B.S. degree from Zhengzhou University, China, in 2012, and the M.S. degree from Guangxi University, China, in 2015. He is currently pursuing the Ph.D. degree with the Institute of Information Science, Beijing Jiaotong University, Beijing, China. His research interests include image processing and digital forensics.

Xiaolong Li received the B.S. degree from Peking University, China, in 1999, the M.S. degree from École Polytechnique, France, in 2002, and the Ph.D. degree in mathematics from ENS Cachan, France, in 2006. From 2007 to 2016, he worked as a Post-Doctoral Fellow and then a Researcher with Peking University. He is currently a Professor with the Institute of Information Science, Beijing Jiaotong University, Beijing, China. His research interests include image processing and information hiding.

Yao Zhao (Senior Member, IEEE) received the Ph.D. degree from the Institute of Information Science, Beijing Jiaotong University (BJTU), Beijing, China, in 1996. He became an Associate Professor with BJTU in 1998 and a Professor in 2001. From 2001 to 2002, he was a Senior Research Fellow with the Information and Communication Theory Group, Faculty of Information Technology and Systems, Delft University of Technology, Delft, The Netherlands. In 2015, he visited the Swiss Federal Institute of Technology (EPFL), Lausanne, Switzerland. From 2017 to 2018, he visited the University of Southern California. He is currently the Director of the Institute of Information Science, BJTU. His current research interests include image/video coding, digital watermarking and forensics, video analysis and understanding, and artificial intelligence. He serves or served on the editorial boards of several international journals, including as an Associate Editor of the IEEE TRANSACTIONS ON CYBERNETICS, an Associate Editor of the IEEE TRANSACTIONS ON CIRCUITS AND SYSTEMS FOR VIDEO TECHNOLOGY, a Senior Associate Editor of the IEEE SIGNAL PROCESSING LETTERS, and an Area Editor of *Signal Processing: Image Communication*. He was named as a Distinguished Young Scholar by the National Science Foundation of China in 2010 and was elected as a Chang Jiang Scholar of the Ministry of Education of China in 2013.

Rongrong Ni received the B.S. and Ph.D. degrees from Beijing Jiaotong University (BJTU), Beijing, China, in 1998 and 2005, respectively. Since 2005, she has been a Faculty with the School of Computer and Information Technology, Institute of Information Science, BJTU, where she has been a Professor since 2013. Her current research interests include image processing, data hiding and digital forensics, pattern recognition, and computer vision.